ADVANCED FUNCTIONAL MATERIALS
www.afm-journal.de

Atomic-Scale Visualization of Polarization Pinning and Relaxation at Coherent $BiFeO_3/LaAlO_3$ Interfaces

Rong Huang, Hang-Chen Ding, Wen-I Liang, Yong-Chao Gao, Xiao-Dong Tang, Qing He, Chun-Gang Duan, Ziqiang Zhu, Junhao Chu, Craig A. J. Fisher, Tsukasa Hirayama, Yuichi Ikuhara, and Ying-Hao Chu**

Complex oxide heterointerfaces, which play host to an incredible variety of interface physical phenomena, are of great current interest in introducing new functionalities to systems. Here, coherent super-tetragonal $BiFeO_3/LaAlO_3$ and rhombohedral $BiFeO_3/LaAlO_3$ heterointerfaces are investigated by using a combination of high-angle annular dark-field (HAADF) imaging and annular bright-field (ABF) imaging in a spherical aberration (Cs) corrected scanning transmission electron microscope (STEM), and first-principles calculations. The complicated ferroelectric polarization pinning and relaxation that occurs at both interfaces is revealed with atomic resolution, with a dramatic change in structure of $BiFeO_3$, from cubic to super-tetragonal-like. The results enable a detailed explanation to be given of how non-bulk phase structures are stabilized in thin films of this material.

1. Introduction

Many unexpected and intriguing properties of complex oxide interfaces have recently propelled these heterosystems to the forefront of materials research.[1,2] Fascinating phenomena can arise from interactions between atoms, their electron orbitals, charges, and spin states which are not found in the bulk materials, resulting in a wide range of properties including colossal magnetoresistance,[3] metal-to-insulator transitions,[4] superconductivity,[5,6] and coupling of lattice instabilities.[7] Concerted theoretical and experimental investigations have been carried out to determine the physical mechanisms underlying these interface interactions in terms of changes in atomic bonding,[8] symmetry breaking, charge transfer, electromagnetic coupling, and strain modulation. The extreme sensitivity of many properties to structural distortions and crystal chemistry also provides various routes to control and engineer new functionalities in these systems.[9] For instance, strain engineering of epitaxial perovskite thin films,[10] as well as controlling charge transfer across the oxide interfaces, has been widely used to obtain high ferroelectric Curie temperatures and polarization in a number of complex oxide thin films by means of epitaxial growth or formation of superlattices.[11–14]

Oxygen atoms provide the backbone of oxide perovskite structures in the form of a corner-shared octahedral network, and play a crucial role in accommodating the crystal lattice mismatch (strain) at a heterogeneous interface. Direct observation of oxygen atoms near such an interface would thus greatly accelerate elucidation of phenomena originating in the structural distortions to the parent lattice this strain induces.

$BiFeO_3$ (BFO) is a promising multiferroic for technological applications and also of immense fundamental interest because its electric polarization is coupled to antiferromagnetic ordering at room temperature, making it possible to manipulate its magnetic properties by application of an electric field,

Dr. R. Huang, H.-C. Ding, Y.-C. Gao, Prof. X.-D. Tang, Prof. C.-G. Duan, Prof. Z. Zhu, Prof. J. Chu, Prof. Y.-H. Chu
Key Laboratory of Polar Materials and Devices
Ministry of Education
East China Normal University
Shanghai, 200062, China
E-mail: cgduan@clpm.ecnu.edu.cn; yinghaochu@gmail.com
Dr. R. Huang, Dr. C. A. J. Fisher, Dr. T. Hirayama, Prof. Y. Ikuhara
Nanostructures Research Laboratory
Japan Fine Ceramics Center
Nagoya, 456–8587, Japan
W.-I Liang, Prof. Y.-H. Chu
Department of Materials Science and Engineering
National Chiao Tung University
Hsinchu, 30010, Taiwan, ROC
Dr. Q. He
Advanced Light Source
Lawrence Berkeley National Laboratory
Berkeley, CA, 94720, USA
Prof. C.-G. Duan, Prof. J. Chu
National Laboratory for Infrared Physics
Chinese Academy of Sciences
Shanghai, 200083, China
Prof. Y. Ikuhara
Institute of Engineering Innovation
the University of Tokyo
Tokyo, 113–8656, Japan

DOI: 10.1002/adfm.201301470

or, conversely, its electrical properties by application of a magnetic field.[15,16] In bulk form, BFO belongs to rhombohedral space group $R3c$ with antiphase octahedral tilting and ionic displacements from the centrosymmetric positions about and along the $<111>_c$ directions (where "c" refers to pseudo-cubic symmetry).[17] When deposited as thin films, however, BFO can take on structural forms not observed in the bulk state due to epitaxial strain from the substrates. Earlier theoretical studies demonstrated that epitaxial strain can stabilize BFO in its tetragonal form with $P4mm$ symmetry, thereby preventing the rotational distortions observed in the $R3c$ bulk phase.[18] When subjected to this constraint, the theoretical ground state of BFO has a massively reduced in-plane lattice parameter of 3.67 Å and a "super-tetragonal" unit cell with c/a = 1.27 (a is the in-plane lattice parameter and c is the out-of-plane lattice parameter). Indeed, a nearly tetragonal phase with an unusually large c/a ratio close to 1.3 has been reported to be stabilized in highly strained BFO films grown on a (001) $LaAlO_3$ (LAO) substrate. LAO has rhombohedral symmetry with a pseudocubic lattice parameter a = 3.79 Å, giving a lattice mismatch of about 4.3% relative to rhombohedral BFO (pseudocubic lattice parameter a = 3.96 Å).[14] Theoretical calculations predict that the tetragonal BFO phase has an enhanced polarization, roughly 1.5 times that of a bulk single crystal,[18] a remarkable increase that has also been confirmed experimentally.[19,20] Also, according to first-principles calculations, by starting from the $P4mm$ symmetry and allowing in-plane polar displacements (along [110]), it may be possible to obtain a monoclinic phase with Cm symmetry that could be more stable,[21,22] a prediction supported by recent experimental results.[13,14,23] A strain-driven rhombohedral (R phase) and super-tetragonal (T phase) mixed phase in BFO thin films grown on LAO substrates has also been reported to exhibit attractive physical properties, namely, electrically controllable spontaneous magnetism.[24] However, despite the importance of the substrate in stabilizing the tetragonal-like BFO (T-BFO) phase, detailed local structures of the BFO/LAO interface, especially the degree of distortion of oxygen octahedra and the source of the ferroelectric polarization, remain unknown, in contrast to the situation for bulk BFO. The lack of such data makes it difficult to explain the stability of the super-tetragonal BFO phase and design strategies for manipulating, optimizing or improving its properties.

Ferroic properties are a sensitive function of the relative positions of anions and cations in the structure, so that quantitative analysis requires identification and characterization of the positions of the light-element atoms, namely oxygen,[25–27] in addition to the heavier metal atoms. Recently, the development of spherical aberration correcting technology (Cs-correction)[28] for transmission electron microscopes (TEM) has markedly improved the spatial resolution of TEM and scanning TEM (STEM) apparatus.[29–33] For example, oxygen columns have been directly imaged in ferroelectric materials with Cs-corrected high-resolution TEM (HRTEM), thereby enabling the origin of their ferroelectric polarization to be identified.[34–37] One drawback of this technique is that it requires preparation of very high quality TEM specimens, usually thinner than 10 nm.

On the other hand, high angle annular dark-filed (HAADF) imaging in a Cs-corrected STEM provides sub-Angstrom resolution and an intuitive image contrast proportional to the atomic number ($\approx Z^2$). It has been widely used to image atom displacements in ferroelectric materials.[13,27,38] However, HAADF-STEM imaging is not sensitive to light elements such as oxygen and nitrogen, especially when heavy elements are also present. Even though octahedral tilts in BFO have been mapped from Z-contrast STEM images, additional image processing was required to do this, and no direct information about individual oxygen columns could be obtained.[25] A more recent development is the annular bright-field (ABF) imaging technique, which can robustly image light elements and heavy elements simultaneously over a wide sample thickness, while still retaining a Z-dependent image contrast ($\approx Z^{1/3}$), within a Cs-corrected STEM.[39,40] Its utility has been demonstrated by the successful imaging of two of the three lightest elements, Li,[41,42] and H.[43,44] In this study, we use ABF imaging to determine the degree of oxygen octahedral distortion near a coherent mixed phase BFO/LAO interface with atomic resolution. Polarization relaxation near both the T-BFO/LAO and R-BFO/LAO interfaces can be ascertained directly by observation of the oxygen column positions.

2. Results and Discussion

BFO thin films were grown on (001) LAO single crystal substrates by pulsed laser deposition. A mixture of the stable super-tetragonal BFO phase with c/a ratio around 1.23, and the distorted rhombohedral BFO phase with c/a ratio around 1.09 was obtained.[24] **Figure 1**a shows a typical ABF image of T-BFO taken along $[100]_c$. The black, dark grey and light grey contrast spots in the image correspond to Bi (Z = 81), Fe (Z = 26), and O (Z = 8) columns, respectively. In-plane displacements of all three constituent atoms of T-BFO can be observed clearly. For example, the Fe columns shift to the upper-left within the rectangles formed by four Bi columns. The leftwards component of these displacements corresponds to in-plane polarization of Fe columns, confirming the Cm symmetry. This is in agreement with previous theoretical investigations[21] showing that the monoclinic T-BFO phase without obvious octahedral tilting (Cm) is favored under large compressive strains.

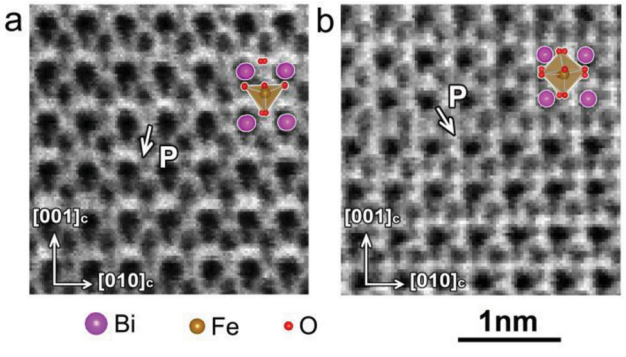

Figure 1. Typical ABF images of a) super-tetragonal $BiFeO_3$, and b) distorted rhombohedral $BiFeO_3$ along the $[100]_c$ zone axis. The atomic structure of both $BiFeO_3$ phases obtained from first-principles calculations is overlaid on the ABF images. The white arrow indicates the polarization direction.

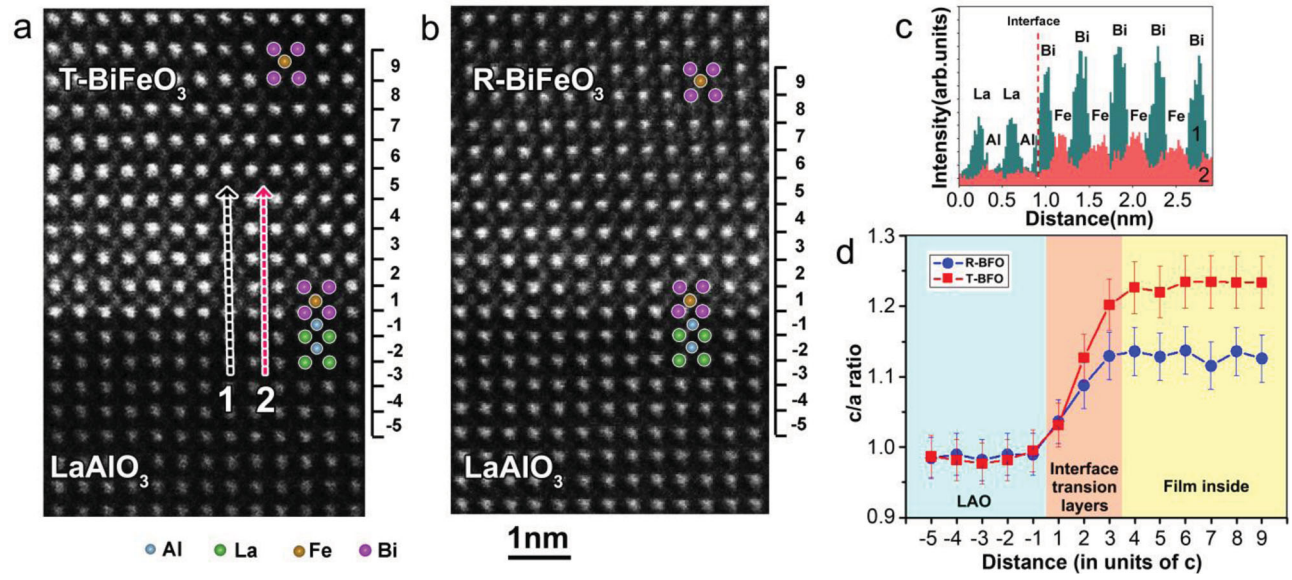

Figure 2. Termination and lattice relaxation of $BiFeO_3/LaAlO_3$ interfaces. a) HAADF image of T-$BiFeO_3/LaAlO_3$ interface along the $[010]_c$ zone axis. b) HAADF image of R-$BiFeO_3/LaAlO_3$ interface along the $[010]_c$ zone axis. c) Image intensity profile along arrows 1 and 2 in (a). d) c/a ratios of T-BFO and R-BFO as a function of distance from the interface.

The *Cm* symmetry allows in-plane polar displacements (along [100]), whose magnitudes depend on the strain level. Further evidence of the in-plane polarization is contained within the positions of the oxygen columns, which match very well with those predicted from first-principles calculations of T-BFO with C*m* symmetry (inset of Figure 1a; see Experimental Section). These also unambiguously show that the Fe ion is bonded to five oxygen atoms to form an Fe-O pentahedron, consistent with recent HAADF-STEM observations.[45] From these structural modifications, a uniquely defined ferroelectric polarization can be calculated, as represented by the white arrow in Figure 1a. Note here that in the T-BFO the off-center displacements of the transition-metal (Fe) atoms (in an almost entirely upwards direction in Figure 1a) occur in the opposite direction to the total ferroelectric polarization (pointing in a downwards direction in Figure 1a), which is the opposite behavior to that of the transition-metal (Ti) atoms in $BaTiO_3$. Figure 1b shows a typical ABF image of R-BFO taken along $[100]_c$. Columns of all three elements, Bi, Fe, and O, can be resolved clearly and match well with the atomic structure of distorted R-BFO (inset of Figure 1b). Fe-O_6 octahedra can be distinguished, as opposed to the Fe-O_5 pentahedra in T-BFO. The out-of-plane lattice vector is inclined about 3° to the left. The Fe columns were shifted to the upper-left inside the Bi frame, corresponding to a lower-right polarization, as represented by the white arrows in Figure 1b. Such observations confirm that ABF imaging is a powerful tool to reveal the type and shape of Fe–O*x* polyhedra and polarization directions in both T-BFO and R-BFO.

Next, we focus on the BFO/LAO interface. **Figure 2**a shows a typical HAADF image of the T-BFO/LAO interface viewed along $[100]_c$. The arrangement of columns of heavier elements, namely Bi, Fe, La, and Al, can be clearly resolved because of the strong *Z*-dependent contrast of HAADF image. The interface is atomically sharp, although oxygen positions cannot be discerned because of a lack of contrast. To determine the atomic terminations of the BFO film and LAO substrate, intensity profiles along arrowed lines 1 and 2 were taken, with the results given in Figure 2c. Profile 1 corresponds to La and Bi columns, and profile 2 to Al and Fe columns. The abrupt decrease in intensity coincides with the position of the interface, and is marked by the dashed line in Figure 2c. We can clearly see that the Bi columns in BFO align with the Al columns in LAO, with an $AlO_2/BiO/FeO_2$ stacking configuration at the interface, confirming that the interface is coherent. Similarly, the R-BFO/LAO interface was observed by HAADF-STEM, as shown in Figure 2b. The same $AlO_2/BiO/FeO_2$ stacking configuration at the interface was revealed. Interestingly, the lattice gradually inclines to the left, indicating a relaxation of the constraint caused by the LAO substrate. This is consistent with the formation of the distorted R-BFO phase.

The in-plane lattice parameter and the out-of-plane lattice parameter can also be measured from the HAADF image. Values of a_{BFO} are very uniform throughout the film, and are similar to that of LAO. However, c_{BFO} increases gradually from the interface to within the film, indicating a drastic relaxation of the lattice in the *c* direction away from the interface. A plot of c/a ratios as a function of distance for both the T-BFO/LAO and R-BFO/LAO interfaces is given in Figure 2d. It shows that the lattice relaxation occurs within a distance of about 3–4 perovskite unit cells (the interface transition layers in Figure 2d). The c/a ratio inside bulk T-BFO is 1.23 ± 0.01, which is slightly smaller than the value of 1.27 (when a = 3.665 Å and c = 4.665 Å) obtained from first-principles calculations.[18] However, the c/a ratio inside bulk R-BFO is 1.13 ± 0.01, much smaller than that of T-BFO. The gap in the c/a ratio between T-BFO and R-BFO can be clearly seen in Figure 2d, consistent with an energy gap between the two, as found by the first-principles calculations.[22]

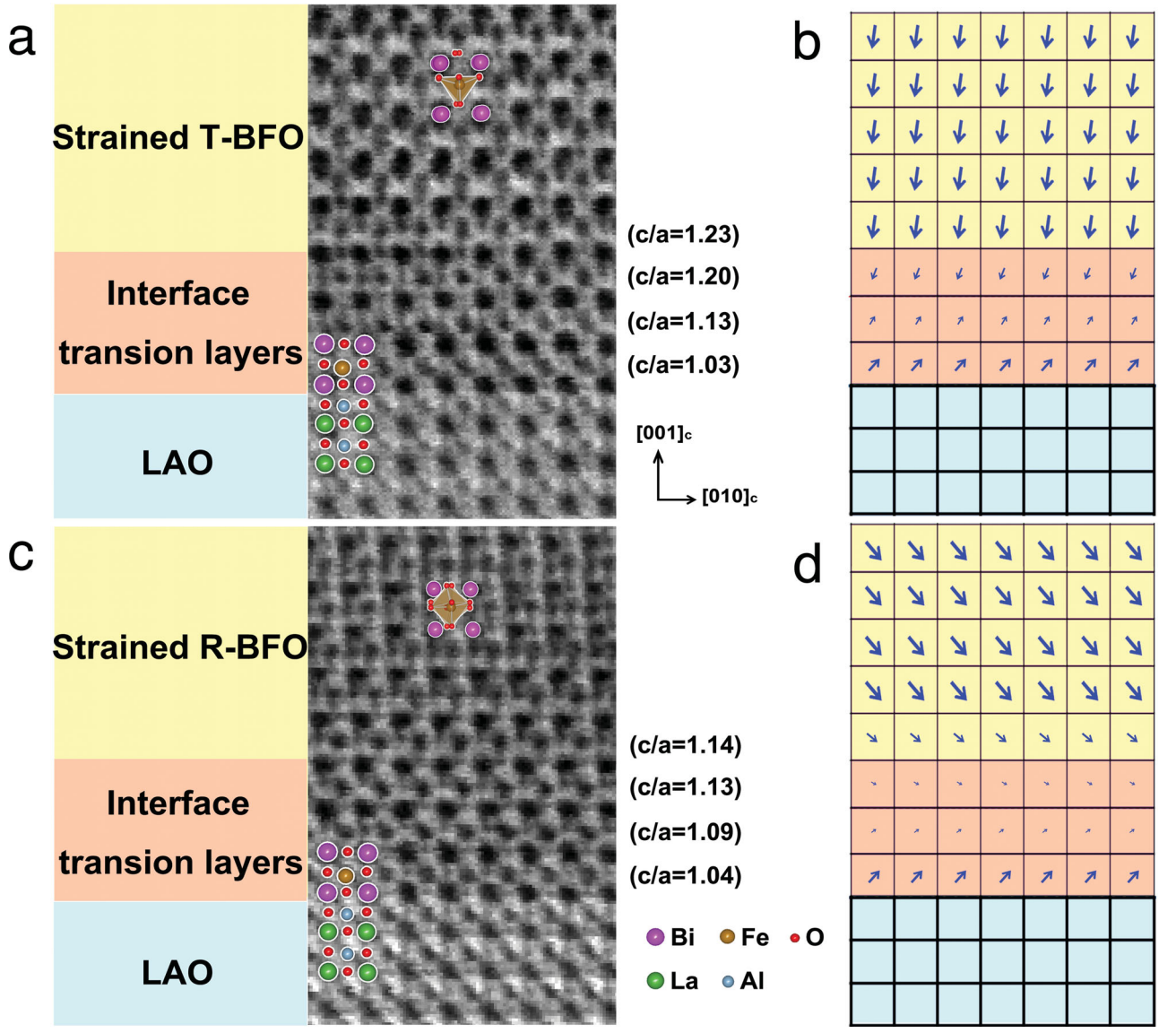

Figure 3. ABF images and polarization pinning diagrams for BFO/LAO interfaces along the $[100]_c$ zone axis and the corresponding polarization relaxation. a) ABF image and b) polarization pinning diagram showing relaxation of T-BFO near the T-BFO/LAO interface. c) ABF image and d) polarization pinning diagram showing relaxation of R-BFO near the R-BFO/LAO interface. The size and direction of the arrows indicate the amplitude and direction of polarization, respectively.

The ferroelectric behavior of the film is undoubtedly related to the nature of the interface termination and lattice relaxation, but the degree of oxygen octahedral distortion and polarization relaxation are perhaps even more important. **Figure 3**a shows an ABF image of the T-BFO/LAO interface along the $[100]_c$ zone axis. The different elemental columns can be distinguished clearly, coinciding well with the overlaid atom structure model, and the interface structure is consistent with that from the HAADF image. In accordance with the increase in the c parameter from the interface upwards, the oxygen octahedra gradually elongate until one oxygen atom becomes separated, eventually resulting in an oxygen pentahedral arrangment around Fe, as shown in Figure 3a.

To determine the polarization of the BFO thin film, displacements of Fe columns from the position at the centre of Bi rectangles were measured. Interestingly, we find that the Fe columns in the first and second BFO monolayers are shifted to the lower-left from the centre of the Bi rectangles by about 0.28 ± 0.11 Å and 0.13 ± 0.07 Å, respectively, corresponding to c/a ratios of 1.03 and 1.13, respectively. This indicates that these two transition layers should be strained R-BFO. However, starting from the third monolayer, the displacement of Fe columns switches to the upper-left, gradually increasing until the column positions correspond to those in the metastable T-BFO structure shown in Figure 1a. According to these ion displacements and oxygen position data, the polarization relaxation at the interface region can be determined, as shown schematically in Figure 3b. The direction and size of the arrows indicate the direction and amplitude of polarization, respectively.

Similarly, the R-BFO/LAO interface was also observed by ABF imaging, as shown in Figure 3c. The interface structure is consistent with that from the HAADF image and with the overlaid structure model. With the increase of the *c* parameter from the interface upwards, the oxygen octahedra gradually begin to tilt, eventually reaching a tilting angle to the left from the perpendicular of about 3° for the strained R-BFO. Interestingly, we find that the Fe columns in the first and second BFO monolayers are shifted to the lower-left from the centre of the Bi rectangles and the displacements are gradually decreased, corresponding to *c*/*a* ratios of 1.04 and 1.09, respectively. This indicates that these two transition layers are also strained R-BFO. However, starting from the third monolayer, the displacement of Fe columns switches to the upper-left, gradually increasing until the column positions correspond to those in the distorted R-BFO structure shown in Figure 1b. This means that the polarization in the first two BFO monolayers is different from that in the rest of the R-BFO thin film, so that the first two monolayers constitute an interface domain. The polarization relaxation at the interface region is shown schematically in Figure 3d. A domain wall (nearly head-to-head) parallel with the interface is revealed which is similar to recent observations by Kim et al.[46]

Based on the above observations, changes in polarization and phase stability can be ascribed unambiguously based on the atomic alignments and concomitant structural relaxation taking place at the T-BFO/LAO and R-BFO/LAO interfaces. The first two BFO monolayers at both interfaces exhibited similar behaviors in terms of lattice relaxation and polarization relaxation, which is most likely a result of interface pinning[47] or charge compensation[37] between the BFO and LAO (or a combination of both). In the case of T-BFO, the strong constraint by the LAO substrate results in a remarkable Fe ion displacement and formation of metastable T-BFO. However, in the case of R-BFO, the substrate strain is at least partially relaxed, so that the strain is lower than the critical strain to form T-BFO, thus maintaining the R-BFO phase, albeit under strain. Furthermore, the first two BFO monolayers in both interfaces are subjected to a nearly hydrostatic strain, which suppresses the tilting of Fe–O_6 octahedra,[48] as shown in Figure 3a,c. Starting from the third BFO monolayer, the polarization pinning effect of the LAO substrate is sufficiently weak to allow the BFO lattice to relax significantly. These large structural relaxations testify to the "softness" of the BFO crystal, accommodating the large strain induced by formation of a coherent interface and achieving energetic stability within a narrow region. This intrinsic lattice flexibility provides opportunities for structure and property tuning through appropriate nanoscale engineering.

To gain a better understanding of the ferroelectric relaxation at the BFO/LAO interface, we also carried out first-principles calculations of BFO with different *c*/*a* ratios within a pseudo-cubic monoclinic basis (see Experimental Sectionfor details). We find that the polarizations of the most stable state in BFO structures are tilted, in accord with experimental observations. Interestingly the state with its in-plane polarization along the [100] direction is more stable than that along the [110] direction. Fixing the in-plane polarization direction to be [100], we plot the magnitude and tilting angle θ of the polarization in BFO with different *c*/*a* ratios in **Figure 4**a. Figure 4a reveals

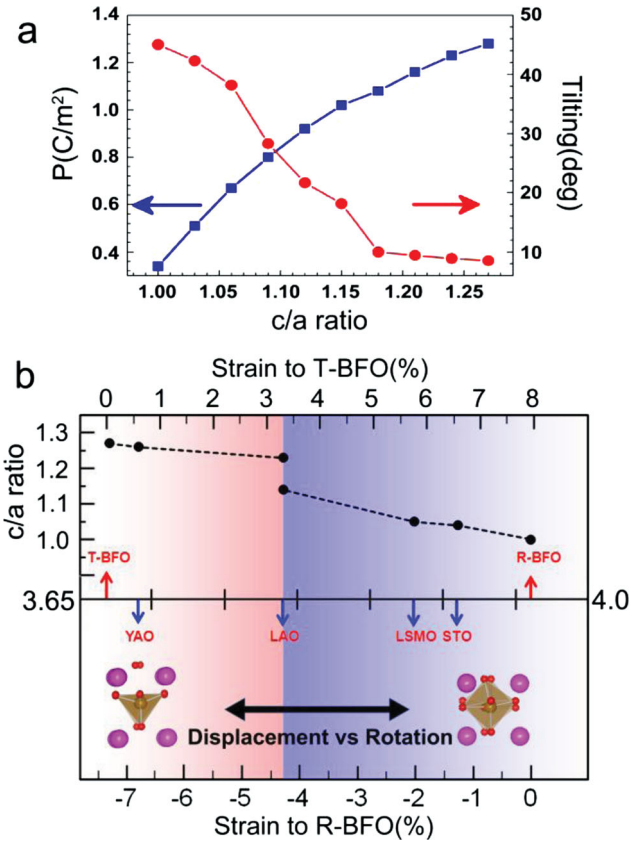

Figure 4. Polarization of BFO and the strain effect on BFO phase stability. a) The magnitude and tilting angle, θ, of the polarization in BFO with different *c*/*a* ratios from first principles calculations. The in-plane polarization is along the [100] direction. b) Substrate strain effect on the stability of T-BFO and R-BFO phases. The competition between displacement of Fe ions and rotation of Fe–O_6 octahedra is dependent on the strain levels and there exists a critial mismatch around –4.3% strain relative to R-BFO. The *c*/*a* ratios of ideal T-BFO, T-BFO on $YAlO_3$, R-BFO on $La_{0.7}Sr_{0.3}MnO_3$ and $SrTiO_3$, and ideal R-BFO were taken from the literature.[13,18,21,26]

that increasing *c*/*a* increases the polarization, and the polarization direction gradually switches to the [001] direction, in agreement with experiment. The calculated giant spontaneous polarization (P = 1.28 C m^{-2}) in the super-tetragonal-like structure (*c*/*a* = 1.27) is also consistent with experiment.[20] In addition, the tilting angle decreases with the increasing of *c*/*a* and shows a different behavior for the rhombohedral-like structure (*c*/*a* less than 1.15) and the tetragonal-like structure (*c*/*a* larger than 1.18).

Figure 4b shows the *c*/*a* ratios of $BiFeO_3$ grown on different substrates, which were taken from the literature.[13,18,21,26] Bulk R-BFO with *c*/*a* = 1.0 was used as a reference for the strained R-BFO phase. Tetragonal $BiFeO_3$ with *P*4*mm* symmetry and *c*/*a* = 1.27 was used as a reference for the strained T-BFO phase. Under an in-plane two dimensional compressive strain (the lower horizontal axis), the *c*/*a* ratio of R-BFO increased and can be tuned continuously. When the mismatch strain reaches –4.3% (corresponding to that induced by the LAO substrate), the T-BFO phase appears. In this case, the *c*/*a* ratio increases

suddenly from ≈1.14 (R-BFO) to ≈1.23 (T-BFO). In contrast, when T-BFO is subjected to an in-plane two dimensional tensile strain (the upper horizontal axis), the c/a ratio decreases gradually and the phase changes to R-BFO at 3.3% strain. In the case of the strained R-BFO, the tilting of Fe–O_6 octahedra is dominant in the structure even though it was suppressed and the displacement of Fe ions was favorable with the increase of compressive strain. However, the displacement of Fe ions (Fe–O_5 pentahedra) is dominant in the strained T-BFO though the tilting of Fe–O_5 pentahedra appears with an increase in tensile strain. Thus, the phase stability of R-BFO and T-BFO is a result of competition between the tilting of Fe–O_6 octahedra and the displacement of Fe ions, as predicted by the first principles calculations.[21]

3. Conclusions

In summary, we have revealed, by means of state-of-the-art ABF and HAADF imaging with a Cs-corrected STEM, that a continuous expansion of the BFO crystal lattice, elongation of oxygen octahedra, and displacement of Fe ions occur at coherent super-tetragonal BFO/LAO and rhombohedral BFO/LAO heterointerfaces. A similar pinned interface transition layer about two unit cells thick was directly observed at both interfaces. The continuous ferroelectric polarization relaxations observed at both T-BFO/LAO and R-BFO/LAO interfaces show very different features, which is a result of competition between the tiliting of Fe–O_6 octahedra and the displacement of Fe ions. Such information is important for rationalizing the varied and complex phenomena of BFO, and adds to our rapidly growing understanding of the ferroelectric behavior of complex oxide heterointerfaces. Additionally, the methods used here are applicable to a wide range of materials, enabling direct observation of atomic structures with unprecedented detail, and should thus further the development of materials nanoscience and nanoengineering.

4. Experimental Section

Pulsed Laser Deposition: The epitaxial BFO thin film containing a mixture of tetragonal and rhombohedra phases was fabricated by pulsed laser deposition in conjunction with high-pressure reflective high-energy electron diffraction from a BFO target with 10% excess bismuth. An $LaAlO_3$ (001) single crystal was used for the substrate. The substrate temperature and oxygen partial pressure were kept at 700 °C and 100 mTorr, respectively, during the deposition. Following deposition, the oxygen partial pressure was increased to 1 atm and the film was cooled to room temperature. More details of the growth conditions and basic characterization methods can be found in an earlier study.[49]

STEM Observation: Cross-sectional TEM specimens were prepared by a standard procedure which included mechanical grinding, polishing, precision dimpling, and ion milling. STEM observations were performed using a Cs-corrected STEM (JEM-2100F, JEOL, Co., Tokyo, Japan) operated at 200 kV and equipped with a spherical aberration corrector (CEOS Gmbh, Heidelberg, Germany), which provided a minimum probe of about 1 Å in diameter. During ABF imaging, a probe convergence angle of 25 mrad and a detection angle of 8–25 mrad were used.

First-Principles Calculations: Total energy calculations were performed within the framework of density-functional theory using the projector augmented wave (PAW) method implemented in the Vienna *Ab Initio* Simulation Package (VASP).[50] The exchange-correlation potential was treated with the generalized gradient approximation (GGA). In case of bulk T-BFO, an energy cut-off of 500 eV was used for the plane wave expansion of the PAWs and a 10 × 10 × 10 Monkhorst-Pack grid for k-point sampling during self-consistent calculations. Structural relaxations were performed until the Hellman-Feynman forces on the relaxed atoms were less than 1 meV $Å^{-1}$. Local orbital-resolved densities of states and local magnetic moments were calculated by projecting the wave functions onto spherical harmonics centred on particular atoms, as implemented in VASP. The in-plane lattice constant of BFO was held fixed at 3.81 Å, which is the theoretical lattice constant of cubic LAO. A pseudocubic monoclinic basis was adopted to simulate the polarization tilting in T-BFO,[22,51] and for different c/a ratios all internal coordinates were fully relaxed to obtain the most stable polarization direction. The Berry phase technique was used to calculate ferroelectric polarizations.[52]

Acknowledgements

The authors thank Dr. Takeharu Kato and Ryuji Yoshida at the Japan Fine Ceramics Center (JFCC) for their help in preparing TEM samples. This work was supported by the National Key Project for Basic Research of China (Grants No. 2013CB922301), NSFC under Grants No. 61125403, PCSIRT, NCET, Shanghai Pujiang talents plan (Grant No. 11PJ1402900), Program of Shanghai Subject Chief Scientist and Fundamental Research Funds for the central universities (ECNU). Computations were performed at the ECNU computing centre. The work at National Chiao Tung University was supported by the National Science Council, R.O.C., under contract No. NSC 101–2119-M-009–003-MY2, Ministry of Education, under grant No. MOE-ATU 101W961, and Center for Interdisciplinary Science of National Chiao Tung University. C.A.J.F. was supported by the Grant-in-Aid for Scientific Research (KAKENHI) "Theoretical Characterization of Heterointerfaces in Thin Films" from the Japan Society for the Promotion of Science.

Received: April 30, 2013
Published online: July 12, 2013

[1] P. Zubko, S. Gariglio, M. Gabay, P. Ghosez, J.-M. Triscone, *Annu. Rev. Condens. Matter Phys.* **2011**, *2*, 141.
[2] M. Bibes, J. E. Villegas, A. Barthelemy, *Adv. Phys.* **2011**, *60*, 5.
[3] Y. Tokura, Y. Tomioka, *J. Magn. Magn. Mater.* **1999**, *200*, 1.
[4] A. Ohtomo, H. Y. Hwang, *Nature* **2004**, *427*, 423.
[5] N. Reyren, S. Thiel, A. D. Caviglia, L. F. Kourkoutis, G. Hammerl, C. Richter, C. W. Schneider, T. Kopp, A. S. Ruetschi, D. Jaccard, M. Gabay, D. A. Muller, J. M. Triscone, J. Mannhart, *Science* **2007**, *317*, 1196.
[6] S. Gariglio, M. Gabay, J.-M. Triscone, *Nat. Nanotechnol.* **2010**, *5*, 13.
[7] N. A. Benedek, C. J. Fennie, *Phys. Rev. Lett.* **2011**, *106*, 107204.
[8] C.-G. Duan, S. S. Jaswal, E. Y. Tsymbal, *Phys. Rev. Lett.* **2006**, *97*, 047201.
[9] W. Eerenstein, N. D. Mathur, J. F. Scott, *Nature* **2006**, *442*, 759.
[10] D. G. Schlom, L.-Q. Chen, C.-B. Eom, K. M. Rabe, S. K. Streiffer, J.-M. Triscone, *Ann. Rev. Mater. Res.* **2007**, *37*, 589.
[11] J. H. Haeni, P. Irvin, W. Chang, R. Uecker, P. Reiche, Y. L. Li, S. Choudhury, W. Tian, M. E. Hawley, B. Craigo, A. K. Tagantsev, X. Q. Pan, S. K. Streiffer, L. Q. Chen, S. W. Kirchoefer, J. Levy, D. G. Schlom, *Nature* **2004**, *430*, 758.
[12] K. J. Choi, M. Biegalski, Y. L. Li, A. Sharan, J. Schubert, R. Uecker, P. Reiche, Y. B. Chen, X. Q. Pan, V. Gopalan, L. Q. Chen, D. G. Schlom, C. B. Eom, *Science* **2004**, *306*, 1005.
[13] R. J. Zeches, M. D. Rossell, J. X. Zhang, A. J. Hatt, Q. He, C. H. Yang, A. Kumar, C. H. Wang, A. Melville, C. Adamo, G. Sheng,

Y. H. Chu, J. F. Ihlefeld, R. Erni, C. Ederer, V. Gopalan, L. Q. Chen, D. G. Schlom, N. A. Spaldin, L. W. Martin, R. Ramesh, *Science* **2009**, *326*, 977.
[14] H. Bea, B. Dupe, S. Fusil, R. Mattana, E. Jacquet, B. Warot-Fonrose, F. Wilhelm, A. Rogalev, S. Petit, V. Cros, A. Anane, F. Petroff, K. Bouzehouane, G. Geneste, B. Dkhil, S. Lisenkov, I. Ponomareva, L. Bellaiche, M. Bibes, A. Barthelemy, *Phys. Rev. Lett.* **2009**, *102*, 217603.
[15] J. Wang, J. B. Neaton, H. Zheng, V. Nagarajan, S. B. Ogale, B. Liu, D. Viehland, V. Vaithyanathan, D. G. Schlom, U. V. Waghmare, N. A. Spaldin, K. M. Rabe, M. Wuttig, R. Ramesh, *Science* **2003**, *299*, 1719.
[16] G. Catalan, J. F. Scott, *Adv. Mater.* **2009**, *21*, 2463.
[17] F. Kubel, H. Schmid, *Acta Crystallogr. Sect. B: Struct. Sci.* **1990**, *B46*, 698.
[18] C. Ederer, N. A. Spaldin, *Phys. Rev. Lett.* **2005**, *95*, 257601.
[19] K. Y. Yun, D. Ricinschi, T. Kanashima, M. Okuyama, *Appl. Phys. Lett.* **2006**, *89*, 192902.
[20] J. X. Zhang, Q. He, M. Trassin, W. Luo, D. Yi, M. D. Rossell, P. Yu, L. You, C. H. Wang, C. Y. Kuo, J. T. Heron, Z. Hu, R. J. Zeches, H. J. Lin, A. Tanaka, C. T. Chen, L. H. Tjeng, Y. H. Chu, R. Ramesh, *Phys. Rev. Lett.* **2011**, *107*, 147602.
[21] B. Dupe, I. C. Infante, G. Geneste, P. E. Janolin, M. Bibes, A. Barthelemy, S. Lisenkov, L. Bellaiche, S. Ravy, B. Dkhil, *Phys. Rev. B* **2010**, *81*, 144128.
[22] A. J. Hatt, N. A. Spaldin, C. Ederer, *Phys. Rev. B* **2010**, *81*, 054109.
[23] H. W. Jang, S. H. Baek, D. Ortiz, C. M. Folkman, R. R. Das, Y. H. Chu, P. Shafer, J. X. Zhang, S. Choudhury, V. Vaithyanathan, Y. B. Chen, D. A. Felker, M. D. Biegalski, M. S. Rzchowski, X. Q. Pan, D. G. Schlom, L. Q. Chen, R. Ramesh, C. B. Eom, *Phys. Rev. Lett.* **2008**, *101*, 107602.
[24] Q. He, Y. H. Chu, J. T. Heron, S. Y. Yang, W. I. Liang, C. Y. Kuo, H. J. Lin, P. Yu, C. W. Liang, R. J. Zeches, W. C. Kuo, J. Y. Juang, C. T. Chen, E. Arenholz, A. Scholl, R. Ramesh, *Nat. Commun.* **2011**, *2*, 255.
[25] A. Borisevich, O. S. Ovchinnikov, H. J. Chang, M. P. Oxley, P. Yu, J. Seidel, E. A. Eliseev, A. N. Morozovska, R. Ramesh, S. J. Pennycook, S. V. Kalinin, *ACS Nano* **2010**, *4*, 6071.
[26] A. Y. Borisevich, H. J. Chang, M. Huijben, M. P. Oxley, S. Okamoto, M. K. Niranjan, J. D. Burton, E. Y. Tsymbal, Y. H. Chu, P. Yu, R. Ramesh, S. V. Kalinin, S. J. Pennycook, *Phys. Rev. Lett.* **2010**, *105*, 087204.
[27] C. T. Nelson, B. Winchester, Y. Zhang, S.-J. Kim, A. Melville, C. Adamo, C. M. Folkman, S.-H. Baek, C.-B. Eom, D. G. Schlom, L.-Q. Chen, X. Pan, *Nano Lett.* **2011**, *11*, 828.
[28] K. W. Urban, *Science* **2008**, *321*, 506.
[29] C. L. Jia, M. Lentzen, K. Urban, *Science* **2003**, *299*, 870.
[30] P. M. Voyles, D. A. Muller, J. L. Grazul, P. H. Citrin, H. J. L. Gossmann, *Nature* **2002**, *416*, 826.
[31] N. Shibata, M. F. Chisholm, A. Nakamura, S. J. Pennycook, T. Yamamoto, Y. Ikuhara, *Science* **2007**, *316*, 82.
[32] P. D. Nellist, M. F. Chisholm, N. Dellby, O. L. Krivanek, M. F. Murfitt, Z. S. Szilagyi, A. R. Lupini, A. Borisevich, W. H. Sides, S. J. Pennycook, *Science* **2004**, *305*, 1741.
[33] P. E. Batson, N. Dellby, O. L. Krivanek, *Nature* **2002**, *418*, 617.
[34] C.-L. Jia, K. W. Urban, M. Alexe, D. Hesse, I. Vrejoiu, *Science* **2011**, *331*, 1420.
[35] C.-L. Jia, V. Nagarajan, J.-Q. He, L. Houben, T. Zhao, R. Ramesh, K. Urban, R. Waser, *Nat. Mater.* **2007**, *6*, 64.
[36] C.-L. Jia, S.-B. Mi, K. Urban, I. Vrejoiu, M. Alexe, D. Hesse, *Nat. Mater.* **2008**, *7*, 57.
[37] M. F. Chisholm, W. Luo, M. P. Oxley, S. T. Pantelides, H. N. Lee, *Phys. Rev. Lett.* **2010**, *105*, 197602.
[38] G. Catalan, A. Lubk, A. H. G. Vlooswijk, E. Snoeck, C. Magen, A. Janssens, G. Rispens, G. Rijnders, D. H. A. Blank, B. Noheda, *Nat. Mater.* **2011**, *10*, 963.
[39] S. D. Findlay, N. Shibata, H. Sawada, E. Okunishi, Y. Kondo, Y. Ikuhara, *Ultramicroscopy* **2010**, *110*, 903.
[40] S. D. Findlay, N. Shibata, H. Sawada, E. Okunishi, Y. Kondo, T. Yamamoto, Y. Ikuhara, *Appl. Phys. Lett.* **2009**, *95*, 191913.
[41] R. Huang, T. Hitosugi, S. D. Findlay, C. A. J. Fisher, Y. H. Ikuhara, H. Moriwake, H. Oki, Y. Ikuhara, *Appl. Phys. Lett.* **2011**, *98*, 051913.
[42] R. Huang, Y. H. Ikuhara, T. Mizoguchi, S. D. Findlay, A. Kuwabara, C. A. J. Fisher, H. Moriwake, H. Oki, T. Hirayama, Y. Ikuhara, *Angew. Chem. Int. Ed.* **2011**, *50*, 3053.
[43] S. D. Findlay, T. Saito, N. Shibata, Y. Sato, J. Matsuda, K. Asano, E. Akiba, T. Hirayama, Y. Ikuhara, *Appl. Phys. Exp.* **2010**, *3*, 116603.
[44] R. Ishikawa, E. Okunishi, H. Sawada, Y. Kondo, F. Hosokawa, E. Abe, *Nat. Mater.* **2011**, *10*, 278.
[45] M. D. Rossell, R. Erni, M. P. Prange, J. C. Idrobo, W. Luo, R. J. Zeches, S. T. Pantelides, R. Ramesh, *Phys. Rev. Lett.* **2012**, *108*, 047601.
[46] Y.-M. Kim, A. Kumar, A. Hatt, A. N. Morozovska, A. Tselev, M. D. Biegalski, I. Ivanov, E. A. Eliseev, S. J. Pennycook, J. M. Rondinelli, S. V. Kalinin, A. Y. Borisevich, *Adv. Mater.* **2013**, *25*, 2497.
[47] C.-G. Duan, R. F. Sabirianov, W. N. Mei, S. S. Jaswal, E. Y. Tsymbal, *Nano Lett.* **2006**, *6*, 483.
[48] M. Guennou, P. Bouvier, G. S. Chen, B. Dkhil, R. Haumont, G. Garbarino, J. Kreisel, *Phys. Rev. B* **2011**, *84*, 174107.
[49] H.-J. Liu, C.-W. Liang, W.-I. Liang, H.-J. Chen, J.-C. Yang, C.-Y. Peng, G.-F. Wang, F.-N. Chu, Y.-C. Chen, H.-Y. Lee, L. Chang, S.-J. Lin, Y.-H. Chu, *Phys. Rev. B* **2012**, *85*, 014104.
[50] G. Kresse, D. Joubert, *Phys. Rev. B* **1999**, *59*, 1758.
[51] H.-C. Ding, C.-G. Duan, *Europhys. Lett.* **2012**, *97*, 57007.
[52] R. D. King-Smith, D. Vanderbilt, *Phys. Rev. B* **1993**, *47*, 1651.